Faculty of Mechanical Engineering
Delft University of Technology

Geometrical Optimisation and Experimental Validation of a Metamaterial to obtain Quasi-Zero-Stiffness

Tom Krom – 5635683, Thomas Paddeu – 5607663, Luc Pijnenburg – 5593344, Florian Simor – 5628733

Abstract

This paper explores quasi-zero-stiffness (QZS) in metamaterials, characterised by a near-flat region in the force-compression graph under specific loads. By utilising linear springs in a slab with an array of staggered dissimilar holes, QZS can be achieved. An energy-based model with torsion and linear springs is optimised and validated through both simulation and experimental methods. Results show how optimised geometries and material combinations enhance the QZS region. This study reveals that it is possible to obtain quasi-zero-stiffness using thermoplastic copolyester and silicone based metamaterials.

Keywords: Metamaterial, Quasi-Zero-Stiffness, Multi-Material Manufacturing, Geometrical Optimisation

1 Introduction

A metamaterial is characterised by its geometry and material composition to alter physical phenomena like sound, light, vibrations and many others [1]. The focus of this paper, quasi-zero-stiffness (QZS) [2, p. 5], is a mechanical property that describes a near-flat section in the force-compression graph of a material under certain load conditions. By exploiting structural behaviour like buckling and linear flexing in a predetermined bi-stable structure, QZS can be feasible.

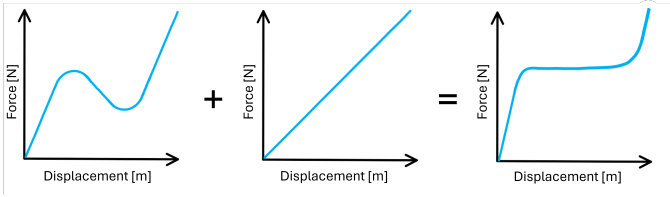

Figure 1: Summation of a bi-stable structure and a linear spring in the force graph creating QZS

QZS is characterised by a plateau in the force-compression graph. This plateau, visible in the third graph of figure 1, translates to having zero stiffness as the stiffness is the derivative of the force to the displacement. The length of the QZS plateau can be maximised by optimising the structure and material parameters. For instance, this metamaterial with a QZS region could be used for vibration isolation [2] for high-precision measurement equipment, allowing more precise and accurate measurements. The length of the QZS plateau needs to be double the amplitude of the vibration in order to isolate it.

This paper will go into detail about how quasi-zero-stiffness can be achieved by optimising a bi-stable geometry combined with linear springs. As a starting point, the geometry and physics simulation are based on a preceding paper [3]. The structure consists of two sets of two, staggered, dissimilar holes, with built-in torsion springs and linear springs. The potential of this shape is already confirmed by extant research [4] - [9]. In this paper, an improved optimisation framework is established. Furthermore, multi-material manufacturing and testing are performed to ensure the model's validity.

2 Methodology

The methodology section goes into depth about the complete optimisation, manufacturing and testing processes of the metamaterial.

2.1 Model optimisation

The energy-based model consists of torsion and linear springs, in combination with a vertically applied force. This model is represented as a linkage as can be seen in figure 2(a). How the linear springs, also referred to as tension bars, are defined is changed to find new useful results. Instead of a connection over the entire model, the tension bars are anchored between the walls of the large holes. Besides that, several other adjustments are made to compensate for earlier miscalculations [3]. Once the model of the metamaterial is improved, the optimisation code is constructed. The previously mentioned geometry, together with its simulated variant can be observed in figure 2.

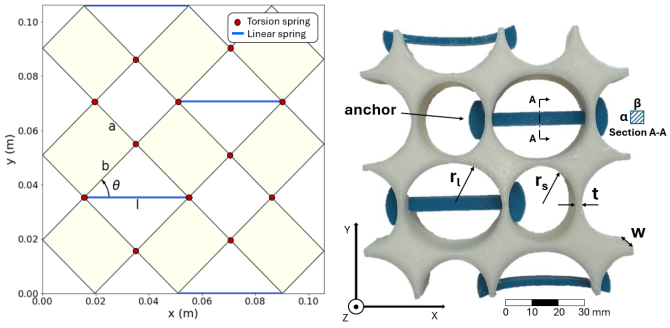

(a) (b)

Figure 2: (a) Linkage model of the geometry, Physical TPC model

The most important model equations are (3) - (6) and are used to calculate and plot the force and stiffness against the compression angle (θ) in figure 2(a). D describes a geometrical parameter required for the torsional calculations [10]. K_t and K_l are the stiffnesses of the torsion spring and tension bar, respectively. P_t and P_l are the potential energy equations for the torsion spring and linear spring.

$$D = \frac{4 r_s r_l}{r_s + r_l} \tag{1}$$

$$h = \frac{\alpha \beta}{d} \tag{2}$$

$$K_t = 0.093 E_b d t^2 \sqrt{\frac{t}{D}} \tag{3}$$

$$K_l = \frac{E_l d h}{r_l} \tag{4}$$

The radii, r_s and r_l, in the first equation relate to the sizes of the small and large holes in the metamaterial. The variable h is defined as the thickness of the tension bar when it extends across the full depth of the metamaterial. The geometrical parameters α and β are used to convert the area of the tension bar to h and the depth, d. The third equation is an approximation based on experimentally gathered data [10]. In the third and fourth equation E_b and E_l represent the Young's moduli of the bulk of the material and that of the tension bar. The parameter t correlates with the thickness of the material between the holes.

$$P_t = 0.5 K_t (\theta - \theta_0)^2 \tag{5}$$

$$P_l = \begin{cases} 0.5 K_l (2b \cos\theta - l_0)^2 & \text{for } l_0 < 2b \cos\theta \\ 0 & \text{otherwise} \end{cases} \tag{6}$$

The parameters in equations (5) - (6) consist of: θ, the length of the tension bar l and a geometric parameter b, as seen in figure 2(a). The compression angle is later substituted for the vertical displacement using trigonometrical relations.

The model optimisation is based on an arbitrarily predefined 0.5% margin [3] around inclination point of the QZS plateau, see figure 3. This margin is singularly used to define the flatness of the QZS plateau. In Appendix A, a closer look is given to the bounds and optimiser used for the optimisation algorithm. A complete overview of the method of optimisation can be found on GitHub [11].

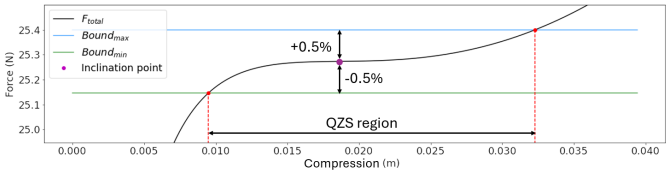

Figure 3: 0.5% force margins from the inclination point as bounds

The geometry can be completely described by seven parameters: r_s, r_l, t, h, w, E_b and E_l. Four of these are optimised: r_s, r_l, t, and h. The depth is fixed as optimising for this variable could negatively influence manufacturability. The Young's moduli are manually selected based on the availability of materials, and the results from the optimisation script. The available materials consist of several types of silicone and plastic.

After completing multiple iterations, the resulting data shows that the force linearly scales with the depth of the material. In the case of silicone, the Young's moduli of the material for the tension bar and the rest of the body should lie as far apart as possible given the possible material options. In consequence, the bulk is made out of the stiffest silicone, 8540. The tension bars are made out of the least stiff silicone, 8510. A second material combination is made using a Thermoplastic copolyester (TPC) (bulk) and silicone 8520 (tension bars). The variables are optimised for both combinations of Young's moduli.

After optimising h, the value was less than the 1 mm casting depth minimum. Therefore, four configurations are made with reduced width, as can be seen in figure 4.

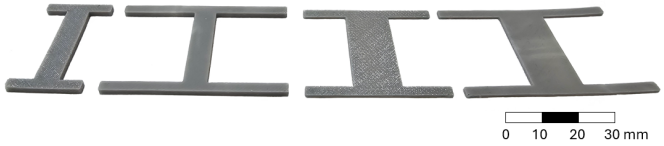

Figure 4: Four configurations of tension bars, from left to right: thick & local flanges, thick & full flanges, thin & local flanges, thin & full flanges

There is a difference in depth which scales inversely with the thickness. Another difference are the local and full flanges to see the influence on the torsion springs. The crux is to keep the area of the tension bar equal to what is calculated in the code.

2.2 Manufacturing

The different material combinations require different manufacturing methods. In the case of a full silicon metamaterial, a double cast is done using two FDM-printed moulds. The tension bars are cast in a flat single-part mould, which is visible in figure 5(a) and a multi-part mould is assembled. After hardening, the tension bars are placed in the cylindrical tension bar holders, visible in the figure of the multi-part mould 5(b). The bulk of the metamaterial is eventually cast around the tension bars. When the silicone has hardened, the metamaterial is carefully taken out of the multi-part mould and cleaned up using a scalpel.

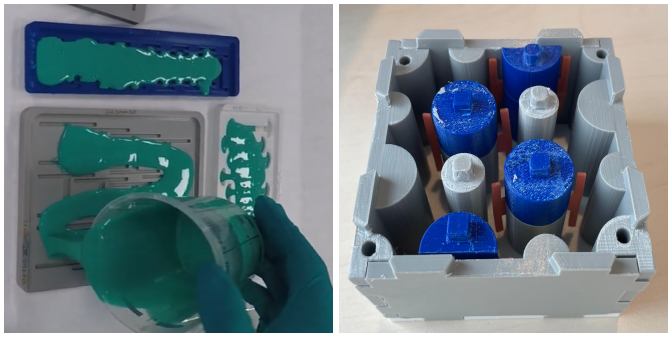

(a) (b)

Figure 5: (a) Casting silicone tension bars, (b) Multi-part mould

The TPC model is 3D-printed at 100% infill. The tension bars for the TPC model are made in a similar way as the ones for the silicone mould. The shape and size of tension bars differ due to the thin walls of the optimised structure. Consequently, the tension bars require an 'anchor' as can be seen in figure 2(b), to hold the tension bars in place. The 3D print stops halfway to insert the tension bars and continues after. The TPC filament has a D45 shore hardness with a Young's modulus of 95 MPa according to the supplier [12].

2.3 Tests

Two different test types are performed to quantify the difference between the theoretical and the practical performance of the metamaterial samples. The tests consist of a standard tensile test at 200 mm/min. For this test, dogbone samples are made to obtain data about the Young's moduli of the silicone material. Before the experimental gathering of the Young's moduli, a first estimation is made to approximate the Young's modulus for the optimisation script [13]. Secondly, a quasi-static compressive test, see figure 6, is performed at 60 mm/min using the metamaterial samples themselves. Resulting in a force-compression diagram for all samples visible in section 3.

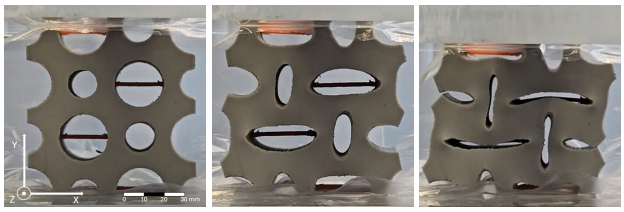

(a) 0 mm (b) 15 mm (c) 25 mm

Figure 6: Compressive test: (a) begin, (b) mid, (c) end

3 Results

The primary result of the experimental validation is the compressive test data. The graph in figure 7 shows the average force-compression response for all metamaterial samples. All of these graphs have been averaged out over three iterations of the compressive experiment. Figure 8 shows the simulated python graphs for the corresponding geometries in figure 7. In figure 9, multiple tests of the same sample can be observed.

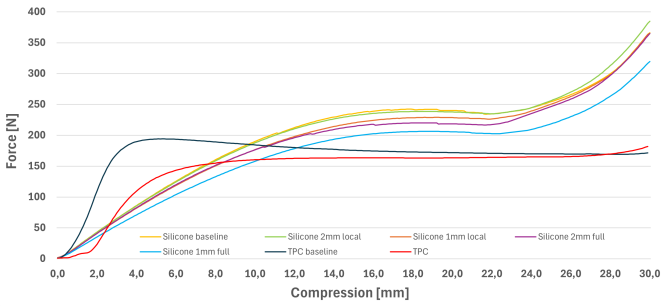

Figure 7: Force-compression graph of TPC and silicone metamaterial test samples

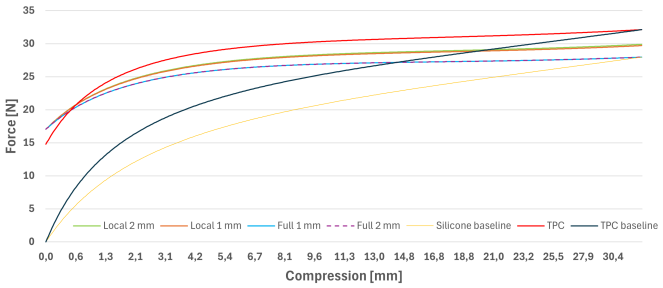

Figure 8: Force-compression graph obtained from python model after adjusting Young's modulus

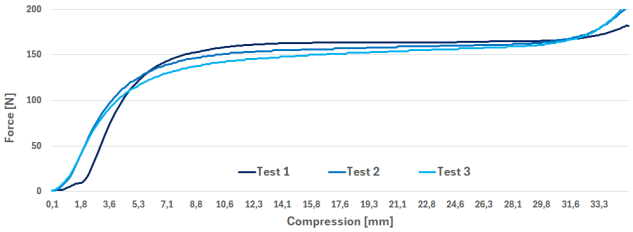

Figure 9: Variation between three compressive tests of a TPC sample

The difference in simulated QZS region percentage and force is described in table 1.

Table 1: Simulated versus tested QZS percentage and corresponding force of the inclination point

Type	Sim value (%)	Test value (%)	Sim force (N)	Test force (N)
Baseline Silicone	2.00	1.00	27.97	238.51
2 mm Local	17.00	6.00	29.02	236.86
2 mm Full	25.00	6.33	27.30	218.55
1 mm Local	17.00	5.33	28.84	227.70
1 mm Full	25.00	3.67	27.30	204.46
Baseline TPC	2.00	1.75	32.13	181.70
TPC	15.00	33.14	31.10	163.37

The comparison between the calculated and test values of the Young's moduli is visible in table 2. The difference between different batches of the same material is shown in table 3.

Table 2: Estimated Young's moduli versus averaged test values

Type	Estimated value (MPa)	Test value (MPA)
Silicone 8510	0.666	0.165
Silicone 8520	0.843	0.241
Silicone 8530	1.066	0.409
Silicone 8540	1.349	0.621
TPC	95*	45.016

* From data sheet [12]

Table 3: Variation in Young's modulus across different batches of bulk silicone type 8540.

Type	Test value (MPa)
2 mm Local	0.619
2 mm Full	0.579
1 mm Local	0.615
1 mm Full	0.579

The optimisation code and test data can be found on GitHub [11].

4 Discussion

This section is divided into two subsections. Firstly, a data analysis where the results are discussed. Secondly, a section to discuss the core issues that were experienced during the project. These points are specified in arbitrary order.

4.1 Data analysis

This analysis is based on data from the compressive test. The most relevant graph is visible in figure 7. It is evident that the TPC force-compression graph is significantly flatter than the silicone metamaterial sample. This is expected to be due to the smaller thickness of the torsion springs resulting in more accurate approximations. The effect of the flatness of

the compressive tests on the quasi-zero-stiffness property is visualised in table 1 with the percentage of the compression that lies within the 0.5% QZS-bounds. It is reasonable for the simulated values to be higher than the test values due to precision issues and friction. In the case of TPC, the tested value is higher than the simulated version. This, together with another prominent difference, the significant differences between the force-compression graph from the simulations and the tests, is visible as the difference between figures 7 and 8. Both of these differences are expected to solely be caused by inaccuracies in the model. Returning to the quasi-zero-stiffness percentages, it is evident that the addition of the tension bars does positively affect the QZS performance of the metamaterial samples. This effect can be seen for both the silicone and the TPC, as both of the baselines show a considerably lower QZS range than the samples with tension bars.

Observing the Young's modulus of each silicone sample and comparing the data with the force-compression graph, a correlation is noticeable between the force and Young's modulus. Combining table 3 and the graph in figure 7, a conclusion can be made that the higher the Young's modulus, the higher the force needed for the same compression. This is confirmed by the simulated force-compression graph 8.

Another observation during testing was the plastic deformation of the TPC samples. This is noticeable in figure 9 by a lower force in the QZS region for every new test. Furthermore, for TPC, viscoelastic effects are also altering the results. This is visible by a less flat QZS region. This effect was resettable by forcing it back or waiting until the TPC sample had retaken its original shape.

4.2 Core issues

The model uses formula (3) that assumes thin walls. In reality, relative to the silicone, the TPC has thinner walls. This explains why the TPC graph is more similar to its simulated version, see figure 7. Furthermore, by the thinner walls of TPC, the bending of the structure plays a more prominent role opposite to the thick walls of silicone where the walls are more compressed than bent.

The definition of the margins in the force graph causes two undesirable effects. The bounds for the QZS are calculated using $1.005F$ and $0.995F$ where F is the force at the inclination point of the graph. Due to this calculation method, the optimiser is biased towards high force metamaterials since the allowed bounds are larger. Next to this, decreasing the 0.5% bound unequally affects the QZS length for different metamaterial samples. Force-compression curves that are flatter towards the centre are impacted less severely by decreasing bounds.

An observation is made during the optimisation phase, namely that a slight change in any of the geometrical parameters correlates with a severe change in simulated behaviour. Because these parameters need to be so precise, it causes problems during manufacturing. Many of the available manufacturing steps do not allow for the extreme precision required, since a deviation of $\mathcal{O}(10^{-4}m)$ can completely negate the calculated QZS-behaviour of the metamaterial.

In the TPC metamaterial, there is a hole in the hinges and in the silicone metamaterial, some of the material has a lower Young's modulus. Therefore, the torsion is most likely lower than calculated and assumed in the model.

The model simulates a four-hole (2x2) geometry, which cannot be linearly scaled to a sixteen-hole (4x4) geometry due to the lack of tension bars between the unit cells. This scaling issue introduces edge effects that diminish with more holes. Additionally, edge effects influence the number of torsion springs, and it is assumed that edge torsion springs are irrelevant. Initially, a sixteen-hole geometry was optimised, but it was altered to a four-hole geometry due to manufacturing and time constraints.

Another important observation regarding the concept of QZS is that it is an inherently unstable feature. The flatter the QZS plateau becomes, the more precision is required for the preload. For a completely flat QZS plateau, infinite precision is required. In the case when the preload does not meet or exceeds the QZS requirement, the material will not function as prescribed.

Another inconsistency lies in the Young's modulus of different samples. Initial rough estimates from silicone and TPC data sheets proved inaccurate by a factor of between two and four during validation via tension tests. Typically, only one dog-bone was made per batch, making results highly sensitive to errors. Even within the same batch, Young's moduli varied from the beginning to the end of the pouring process. Additionally, the non-linearity of elastomer Young's moduli, which depend on strain, further complicates accurate estimations.

5 Conclusion

This paper investigated the development of quasi-zero-stiffness in multi-material metamaterials through optimization, manufacturing, and testing. QZS was realized and optimized using various geometric and material parameters. Silicone and TPC materials are utilised. Testing reveals significant differences between theoretical and practical performance. The results confirmed the positive impact of tension bars on QZS performance, although manufacturing precision and material inconsistencies presented challenges. Despite these issues, the study has shown a proof of concept for QZS metamaterials.

Acknowledgement

We would like to express our gratitude to Freek Broeren and the PME lab technicians for their invaluable contributions throughout this research endeavour.

Bibliography

[1] "A definition | Center for Metamaterials and Integrated Plasmonics." https://metamaterials.duke.edu/definition

[2] X. Zhang, X. Lu, C. Li, R. Tian, L. Chen, and M. Wang, "Design of hyperbolic quasi-zero-stiffness metastructures coupled with nonlinear stiffness for low-frequency vibration isolation," *Engineering Structures/Engineering Structures (Online)*, vol. 312, p. 118262, Aug. 2024, doi: 10.1016/j.engstruct.2024.118262.

[3] Pijpers, M.G. "Metamaterials: An interesting approach to damping".

[4] K. Bertoldi, M. C. Boyce, S. Deschanel, S. M. Prange, and T. Mullin, "Mechanics of deformation-triggered pattern transformations and superelastic behavior in periodic elastomeric structures," Journal of the Mechanics and Physics of Solids/Journal of the Mechanics and Physics of Solids, vol. 56, no. 8, pp. 2642–2668, Aug. 2008, doi: 10.1016/j.jmps.2008.03.006.

[5] J. T. B. Overvelde, S. Shan, and K. Bertoldi, "Compaction through buckling in 2D periodic, soft and porous structures: effect of pore shape," Advanced Materials, vol. 24, no. 17, pp. 2337–2342, Mar. 2012, doi: 10.1002/adma.201104395.

[6] F. G. Broeren, V. Van Der Wijk, and J. L. Herder, "Spatial pseudo-rigid body model for the analysis of a tubular mechanical metamaterial," Mathematics and Mechanics of Solids, vol. 25, no. 2, pp. 305–316, Sep. 2019, doi: 10.1177/1081286519875500.

[7] J. Shim et al., "Harnessing instabilities for design of soft reconfigurable auxetic/chiral materials," Soft Matter, vol. 9, no. 34, p. 8198, Jan. 2013, doi: 10.1039/c3sm51148k.

[8] T. Mullin, S. Deschanel, K. Bertoldi, and M. C. Boyce, "Pattern transformation triggered by deformation," *Physical Review Letters*, vol. 99, no. 8, Aug. 2007, doi: 10.1103/physrevlett.99.084301.

[9] B. Florijn, C. Coulais, and M. Van Hecke, "Programmable mechanical metamaterials," Physical Review Letters, vol. 113, no. 17, Oct. 2014, doi: 10.1103/physrevlett.113.175503.

[10] JPE, "Flexure hinge or elastic hinge - JPE," *JPE*, Jul. 20, 2020. https://www.jpe-innovations.com/precision-point/flexure-hinge-elastic-hinge/

[11] FlorianSimorTU, "GitHub - FlorianSimorTU/BEP-Metamaterial: Code of the geometrical optimisation of a metamaterial to obtain quasi-zero-stiffness.," GitHub. https://github.com/FlorianSimorTU/BEP-Metamaterial

[12] "RS PRO 1.75mm Natural FLEX 45 3D Printer Filament, 500g | RS." https://nl.rs-online.com/web/p/3d-printing-materials/8320523

[13] H. J. Qi, K. Joyce, and M. C. Boyce, "Durometer hardness and the Stress-Strain behavior of elastomeric materials," *Rubber Chemistry and Technology*, vol. 76, no. 2, pp. 419–435, May 2003, doi: 10.5254/1.3547752.

[14] Wikipedia contributors, "Lipschitz continuity," *Wikipedia*, Jun. 04, 2024. https://en.wikipedia.org/wiki/Lipschitz_continuity

[15] "scipy.optimize.basinhopping — SciPy v1.13.1 Manual." https://docs.scipy.org/doc/scipy/reference/generated/scipy.optimize.basinhopping.html

[16] "minimize(method='trust-constr') — SciPy v1.13.1 Manual." https://docs.scipy.org/doc/scipy/reference/optimize.minimize-trustconstr.html

A Python and calculations

Bound definition

The bounds for the four optimised values are based on manufacturing and structural limits. The lower limit for t (the space between the holes) is set at 1 mm due to manufacturing constraints, while the upper limit is 1 cm to exclude thick-walled structures. For the cross-sectional area of the tension bar, the lower limit is 1 mm by 5 mm to ensure structural integrity. The holes' radii are bounded between 5 mm and 5 cm to control the total size of the metamaterial (2x2 and 4x4 holes). These bounds are normalised to ensure the basin-hopping optimiser functions correctly. Normalisation prevents large differences in parameter sizes, which can otherwise cause disproportionate changes during optimisation due to the 'temperature' parameter.

Optimiser choice

The cost function is expected to be smooth with spikes from added penalties, thus not Lipschitz continuous [14], which hinders the convergence of many global optimisation methods. Therefore, Basin-hopping [15] is used. This method involves guessing a random point within set bounds and applying a local optimisation method (trust-constraint optimiser [16]) to validate guesses. This combination efficiently finds the global minimum and aligns well with the model.

Young's modulus

This section will explain how the average Young's modulus of a dogbone sample is calculated. All formulas, data, and plots can be found on GitHub [11].

First, the crossectional area, A_d, and the initial length of the neck of the dogbone, l_0 are measured. Then the tensile test is executed. The tensile test returns force, F, and displacement, l, data. Via equation (7), the Young's modulus for every step is calculated.

$$E = \frac{Fl}{A_d l_0} \tag{7}$$

An average is made from the values that lie in the range of the compressive test values since that is the range of motion of the metamaterial. The tensile test graph of silicone and polymers starts non-linear. The range of motion lies in that non-linear region and therefore the calculated average is a rough estimation. More advanced tests must be done to find a more exact value for the Young's modulus.

B Figures

All relevant and important graphs not used in the paper are listed below:

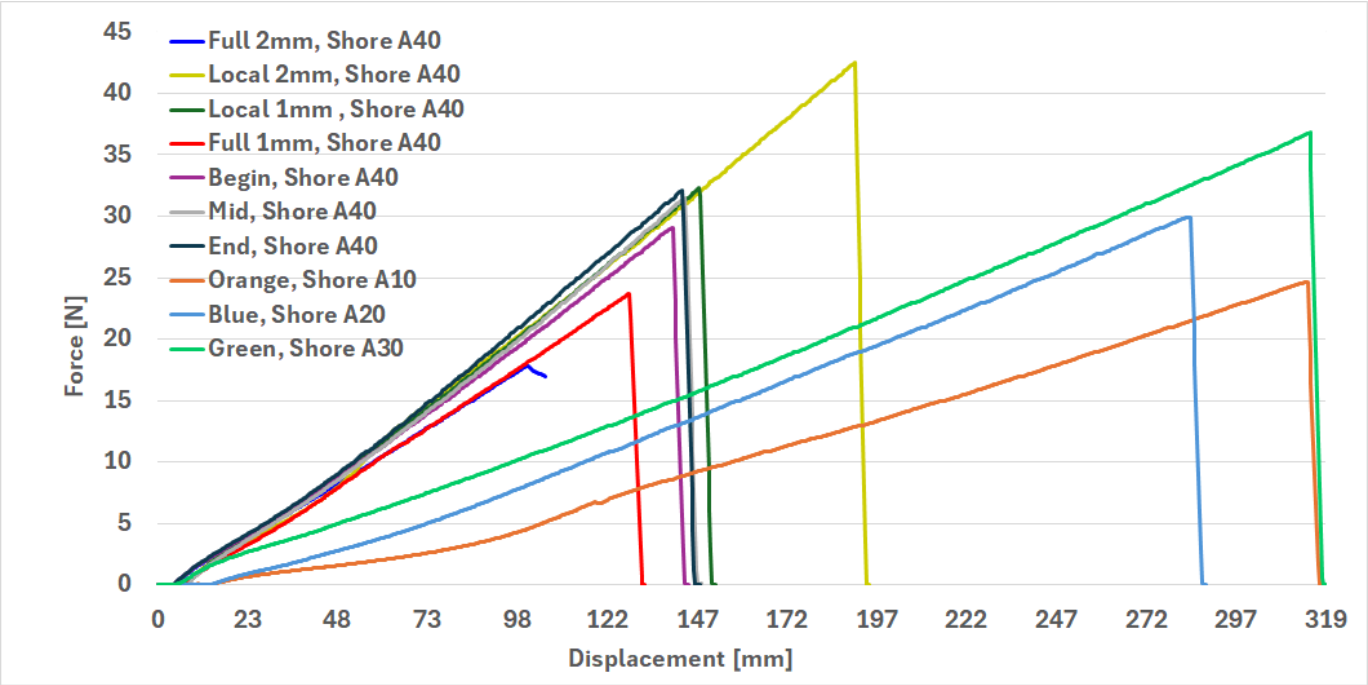

Figure 10: Force-compression graph of tensile test measurements of all silicone dogbone samples

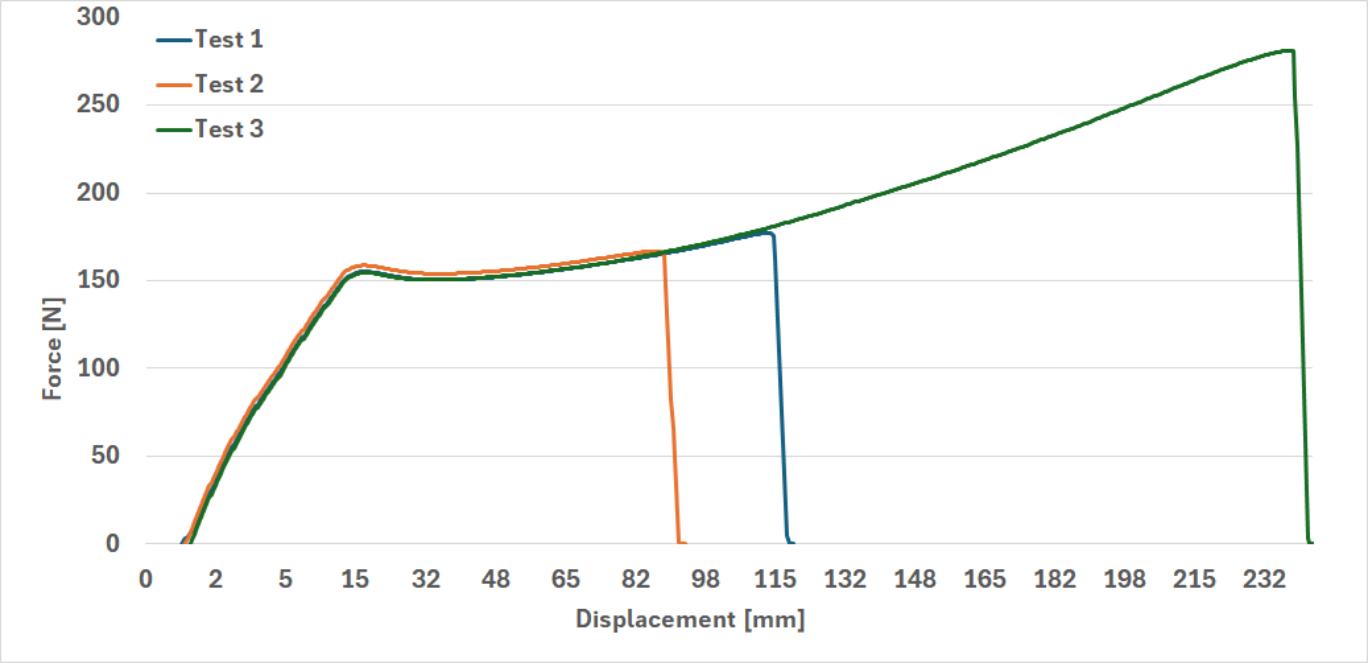

Figure 11: Force-compression graph of tensile test measurements of all TPC dogbone samples

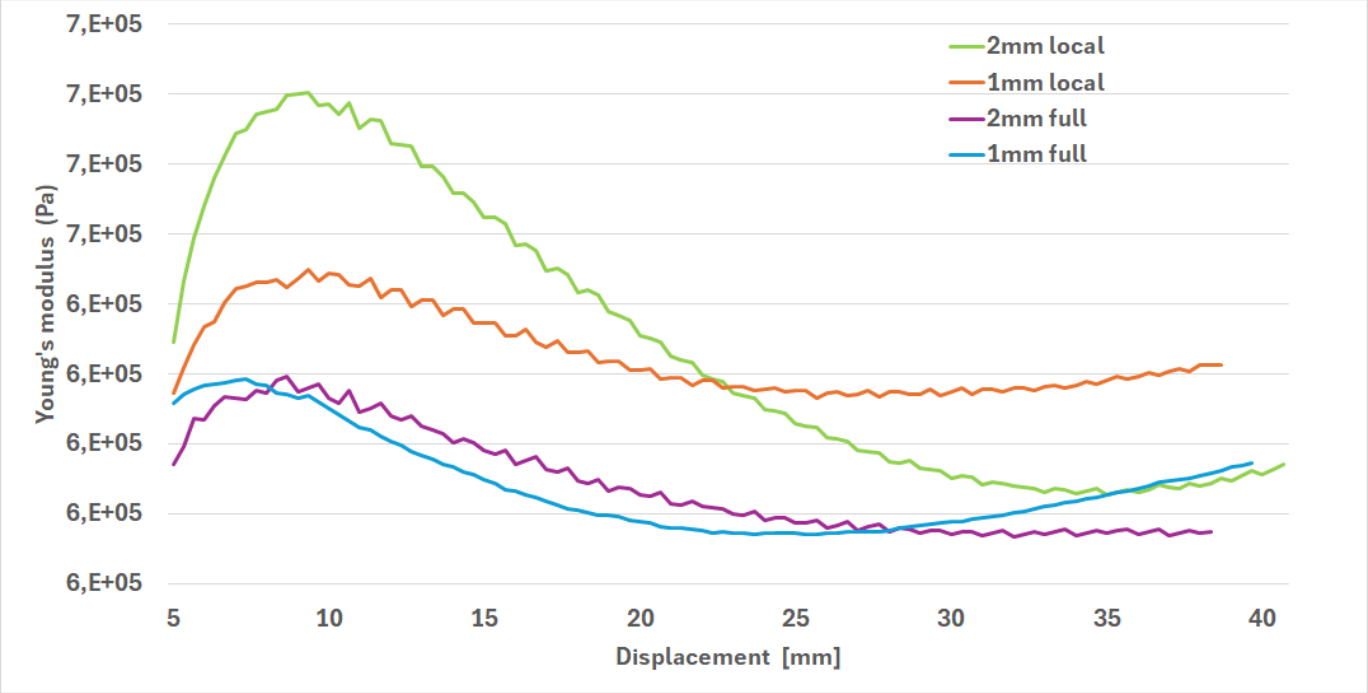

Figure 12: Young's modulus-displacement graph of the silicone bulk, shore A40

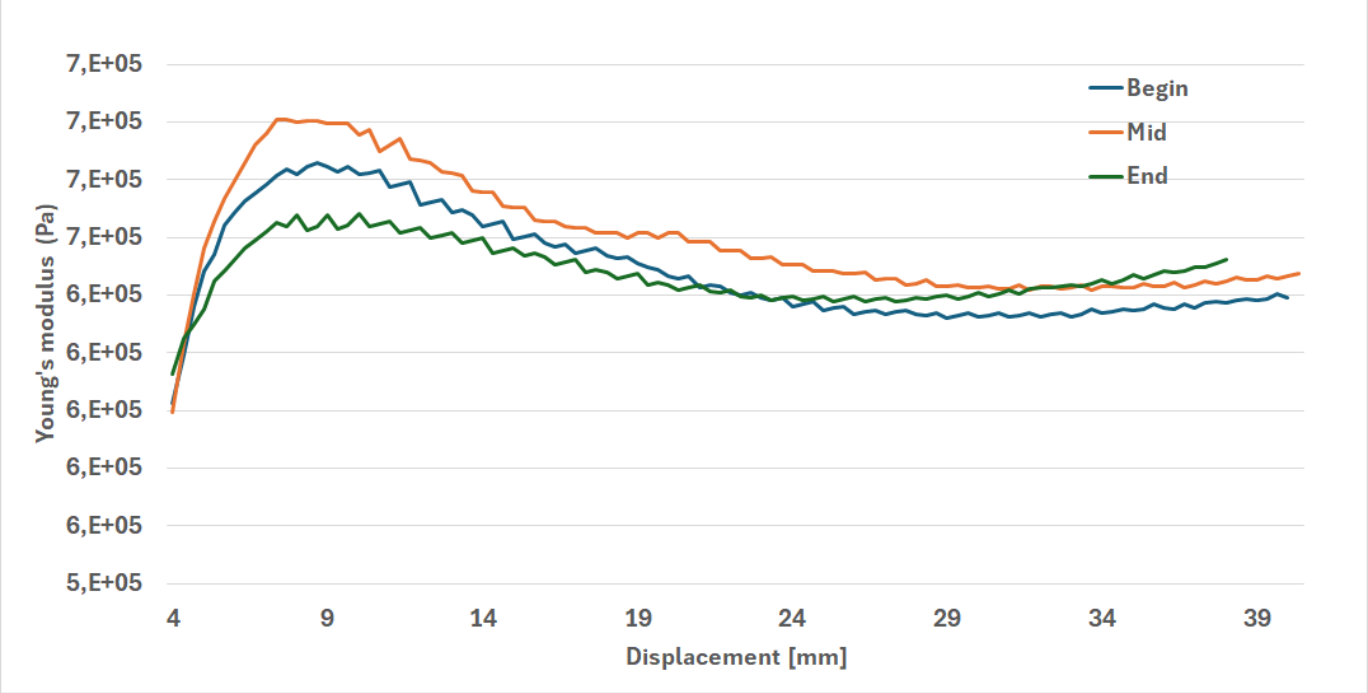

Figure 13: Young's modulus-displacement graph of tension bars with shore A40 during begin, mid and end of the pouring process

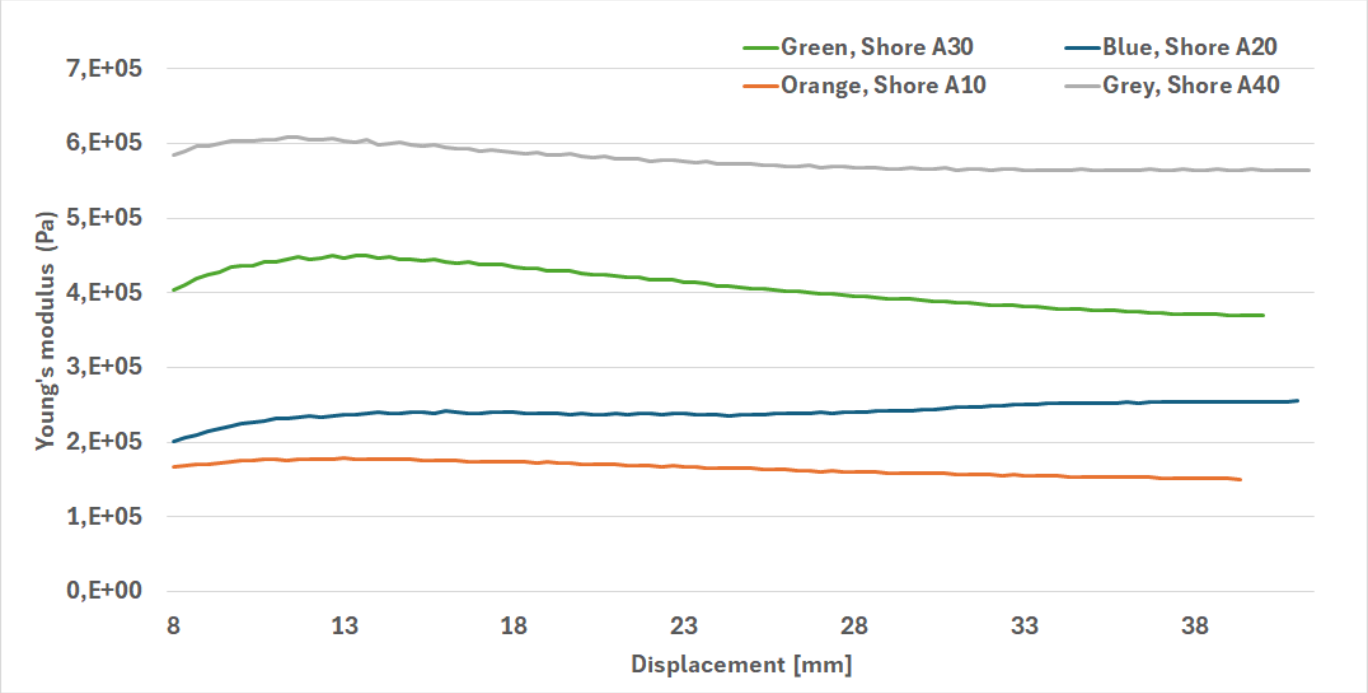

Figure 14: Averaged Young's modulus-displacement graph of the different silicone types

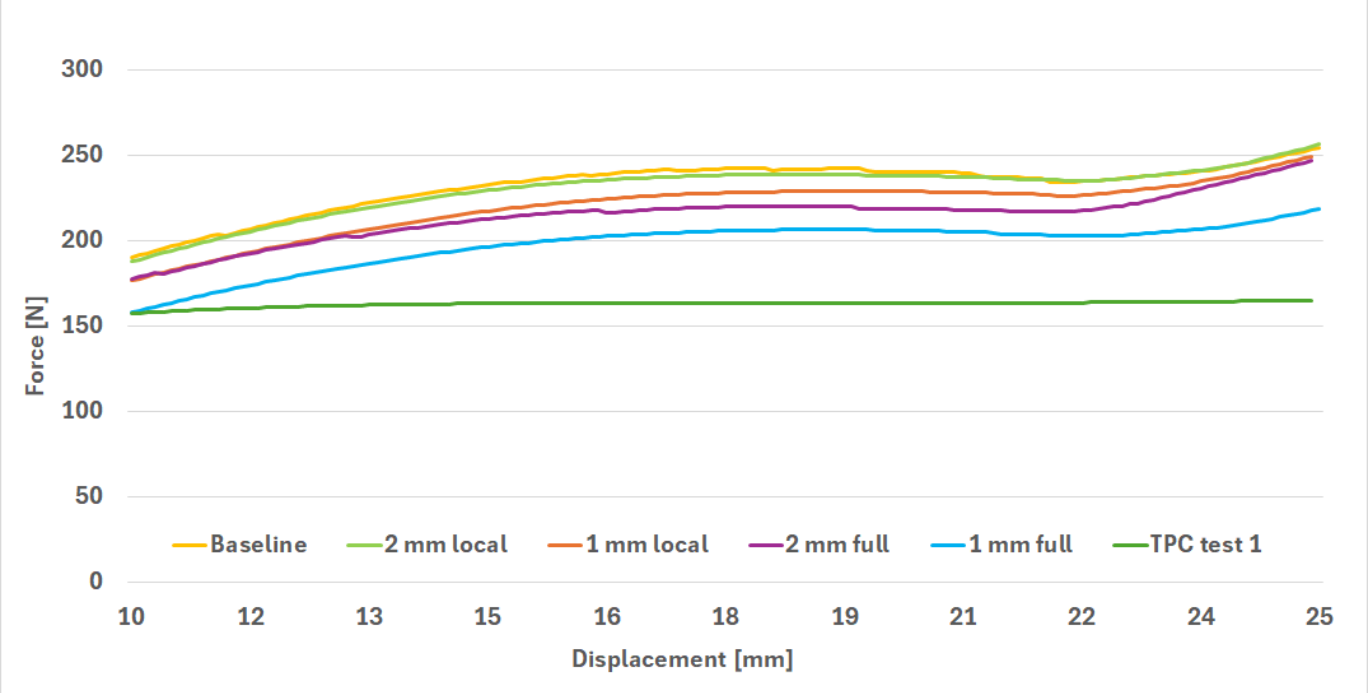

Figure 15: Force-compression graph of the silicone samples zoomed in on the QZS region

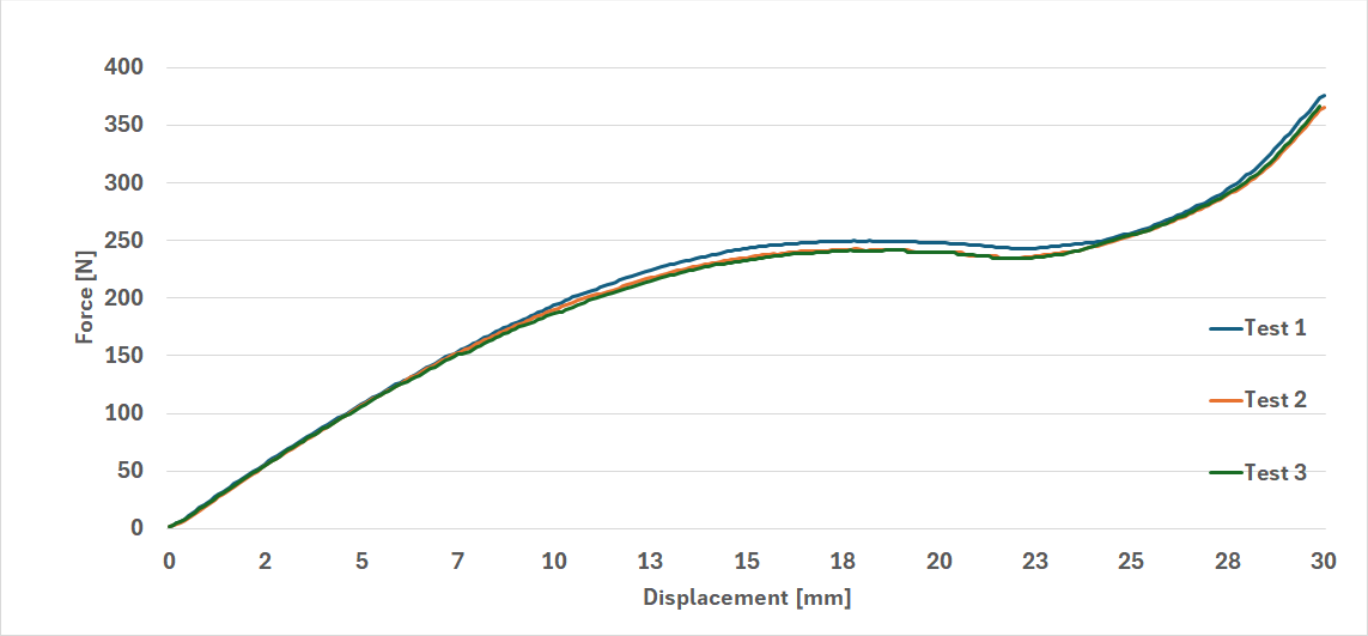

Figure 16: Force-compression graph of the silicone sample without tension bars

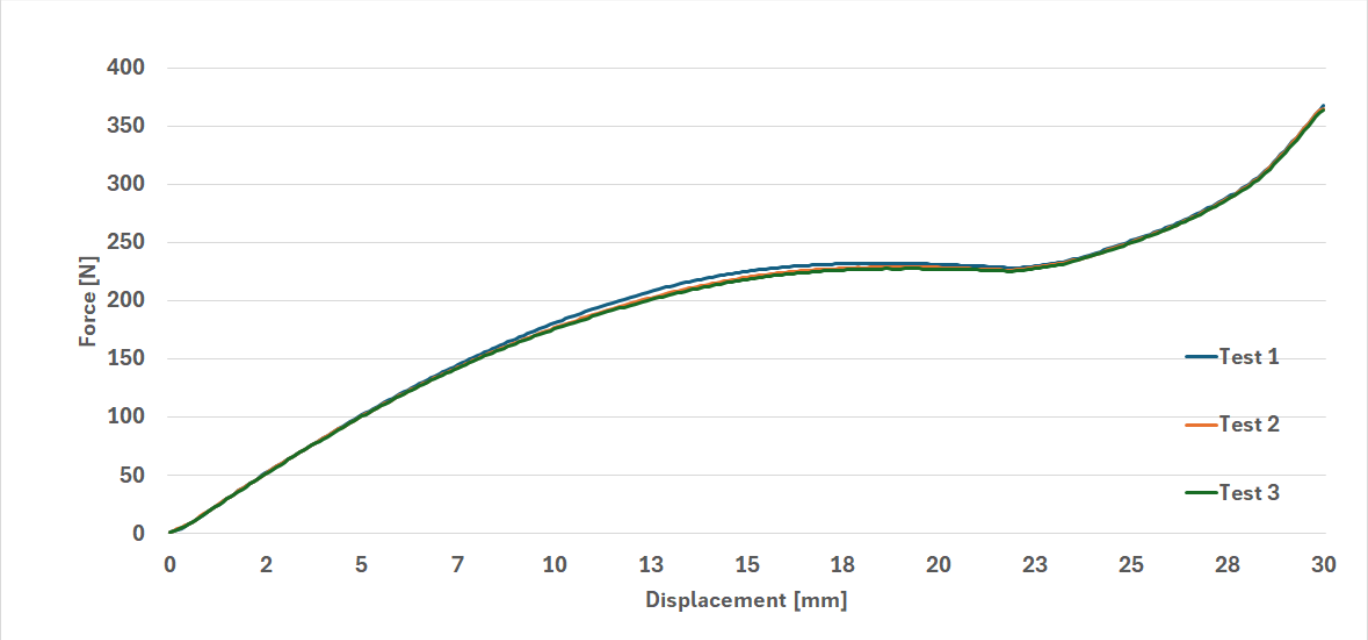

Figure 17: Force-compression graph of the silicone sample with the 1 mm local tension bars

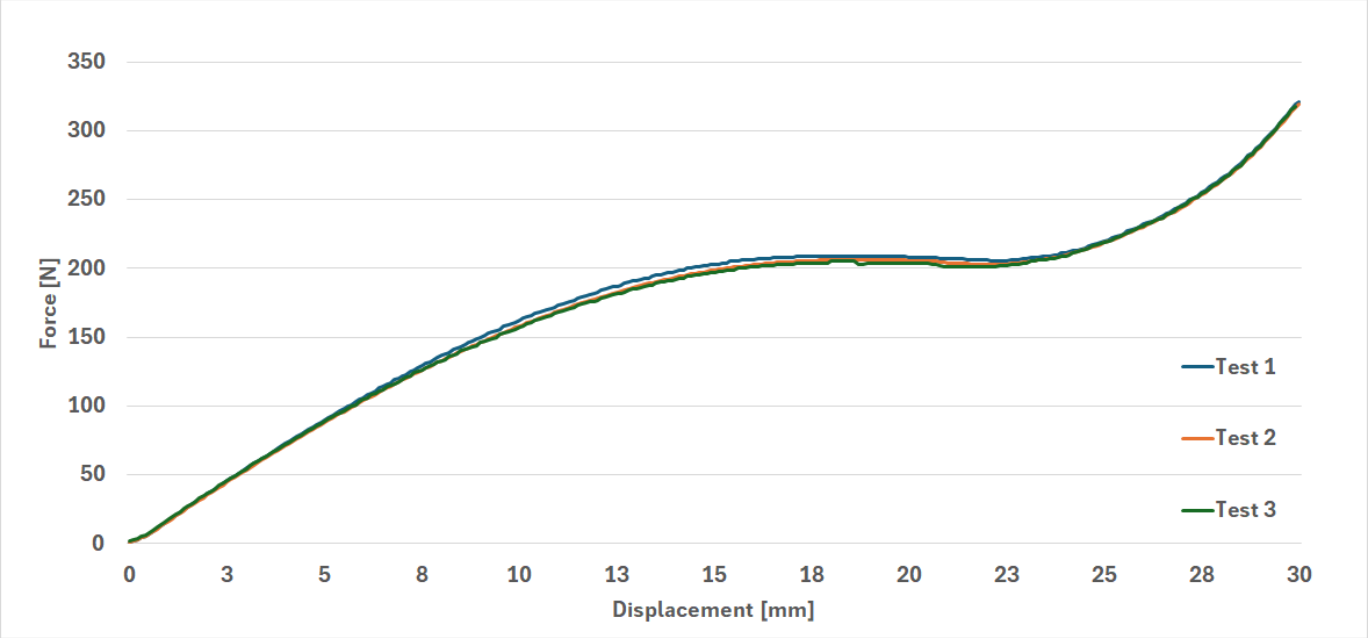

Figure 18: Force-compression graph of the silicone sample with the 1 mm full tension bars

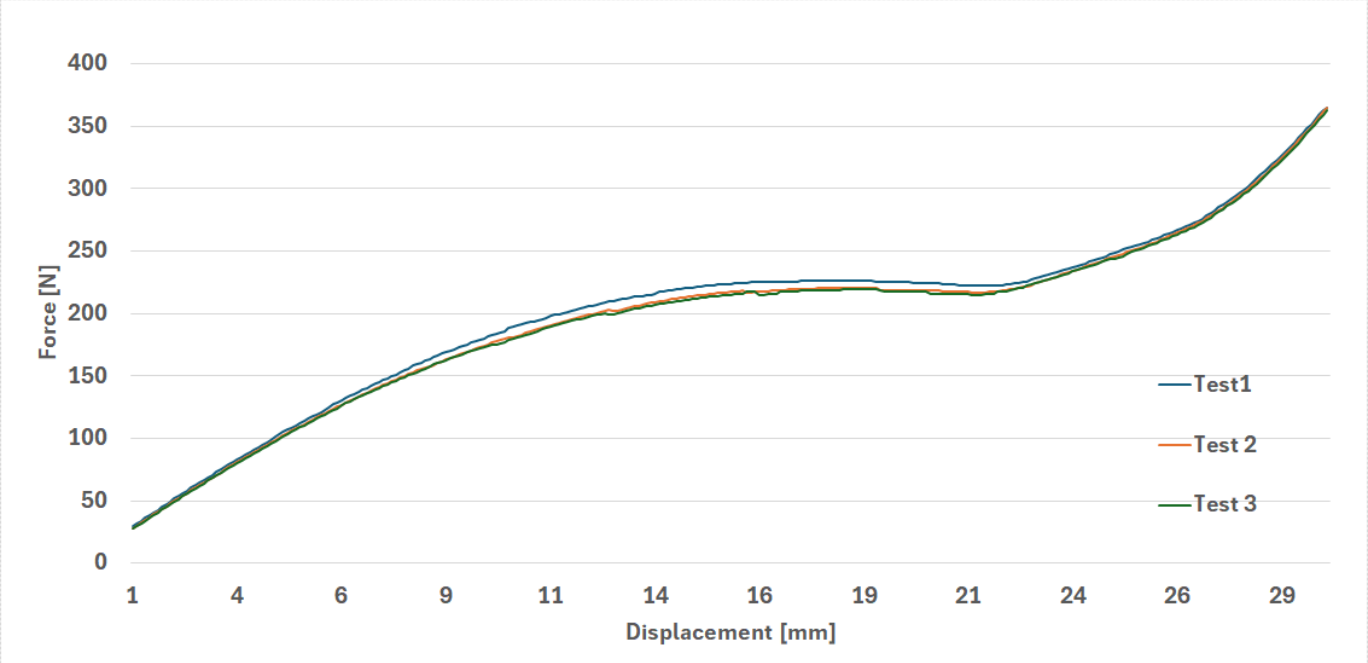

Figure 19: Force-compression graph of the silicone sample with the 2 mm full tension bars

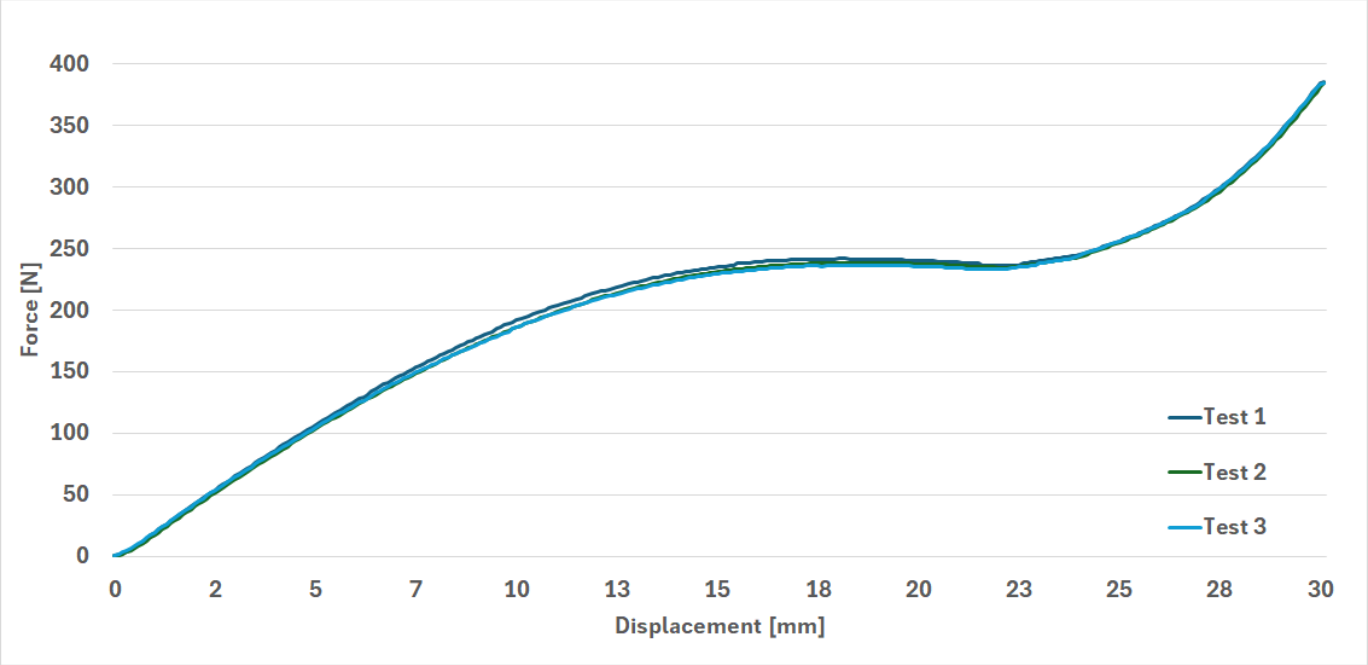

Figure 20: Force-compression graph of the silicone sample with the 2 mm local tension bars

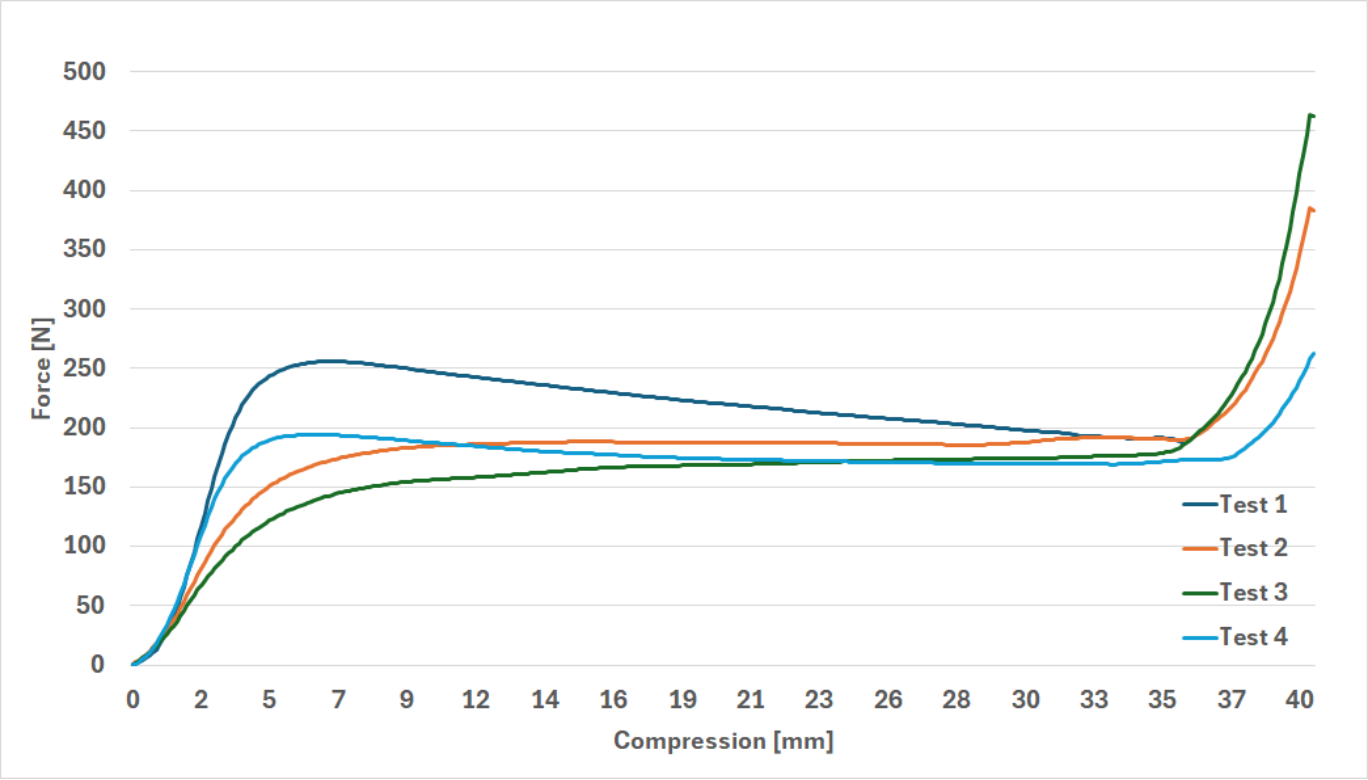

Figure 21: Force-compression graph of the TPC sample without tension bars